JOURNAL OF CATALYSIS 150, 18–33 (1994)

One-Step Synthesis and Characterization of Zirconia–Sulfate Aerogels as Solid Superacids

David A. Ward and Edmond I. Ko[1]

Department of Chemical Engineering, Carnegie Mellon University, Pittsburgh, Pennsylvania 15213

Received April 25, 1994; revised June 30, 1994

Zirconia–sulfate (ZrO_2–SO_4^{2-}) aerogels were prepared in a one-step synthesis by the sol–gel method followed by supercritical drying. Sulfuric acid was mixed with zirconium *n*-propoxide in *n*-propanol and reacted with water and nitric acid to form a zirconia–sulfate cogel. Supercritical drying with carbon dioxide removed the alcohol solvent forming a high surface area aerogel. This preparation method combined the two steps of zirconia support formation and sulfate promotion. The effect of changing sulfate content and activation temperature was systematically studied by nitrogen adsorption, X-ray diffraction, *n*-butane isomerization, diffuse reflectance infrared spectroscopy, pyridine adsorption, and thermogravimetry. Sulfate ions, in an ionic, inactive low temperature state, were initially trapped in the bulk of the aerogel. Coincident with crystallization of the zirconia support, sulfate was expelled onto the surface and transformed into an "activated" covalent sulfate species which helped to form strong Brønsted acidity. A minimum density of sulfate groups was required to create this Brønsted acidity which was necessary for *n*-butane isomerization. Increasing sulfate content retarded the support crystallization and increased the activation temperature required to generate maximum catalytic activity. This aerogel synthesis permitted unique preparative flexibility allowing for sulfate to be introduced into the bulk and for crystallization to be retarded to high temperatures, thus establishing the relationship between crystallinity, sulfate structure and content, and the acidity and activity of the catalyst. This work demonstrated the importance of the preparative parameters on the formation of a solid superacid.

INTRODUCTION

Solid superacids are an important class of catalysts. Superacids, defined as materials with an acid strength stronger than 100% sulfuric acid (1), have many benefits such as the ability to lower reaction temperatures and to form reaction intermediates unattainable with conventional acid catalysts. Most superacids currently in use are homogeneous liquid catalysts, which present many problems. Liquid catalysts are difficult to separate from the product stream. Large amounts of catalyst are usually required, often leading to wasted catalyst. Furthermore, the liquid acids are corrosive to the reactive system and the liquid waste is an environmental hazard. A solid superacid catalyst circumvents many of these problems (1).

One particular type of potential solid superacid is sulfate-promoted zirconium oxide (zirconia). It was first reported in 1979 by Hino *et al.* (2) as a catalyst for the room temperature isomerization of *n*-butane. Low temperature isomerization is of interest to the petroleum industry as branched alkanes are becoming an important product for use as octane-enhancing additives to gasoline. A solid superacid catalyst would lower the reaction temperature required for the isomerization. A lower reaction temperature not only represents an energy savings, but also favors the desired branched product thermodynamically (3). Sulfate-promoted zirconia has also been shown to be active for a number of other reactions including cracking, alkylation, and esterification (4).

The two most common routes for preparing sulfate-promoted zirconia are immersing zirconium hydroxide in a dilute solution of sulfuric acid and impregnating zirconium hydroxide with a solution of ammonium sulfate to incipient wetness. Other methods have been used such as gaseous impregnation with H_2S or SO_2 (5). The effect of sulfate promotion on the physical and textural properties of the catalyst has been examined. Sulfate promotion generally has been found to inhibit the sintering and surface area decrease of zirconia upon heat treatment (5–10). Its effect on the crystal structure evolution of the zirconia support has been studied by X-ray diffraction (5–11) and differential thermal analysis (6, 7, 12).

To understand how sulfate promotion generates superacidity, studies have been performed to determine the structure of the sulfate species on the surface of these materials. Using infrared spectroscopy and X-ray photoelectron spectroscopy, Tanabe and co-workers (13, 14) proposed a chelating bidentate structure. In the presence of water (see Fig. 1a), this structure was very similar to inorganic sulfate complexes. Removal of water transformed the sulfate structure closer to an organic sulfate

[1] To whom correspondence should be addressed.

0021-9517/94 $6.00

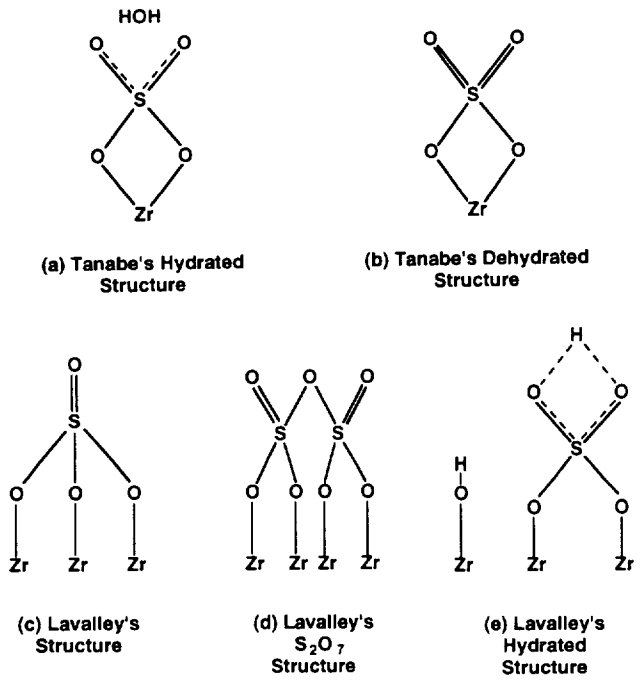

FIG. 1. Proposed structures for the sulfate ion on sulfate-promoted zirconia. (a) and (b) are from Refs. (13) and (14), (c)–(e) are from Refs. (15) and (16).

with a stronger covalent character to the S=O double bonds (see Fig. 1b). They proposed that this structure generated superacidity by the electron inductive effect of the S=O double bonds, increasing the electron deficient nature of the metal atom attached to the sulfate group. This effect strengthened the Lewis acid character of the metal atom. Sohn and Kim (5) agreed with this structural assignment.

In contrast, Lavalley and co-workers (15, 16) proposed a different structure (henceforth denoted as Lavalley's structure for brevity) with only a single S=O double bond with the sulfur atom anchored to the oxide surface through three S–O–Zr linkages (see Fig. 1c). In a dehydrated state, they reported three different sulfate species. At low sulfate coverage, two separate species existed with the above single S=O double bond structure. These two species were differentiated by their location on different crystal faces of the zirconia support. At higher sulfate loadings, a third species formed. This species was thought to be a polysulfate structure like S_2O_7 (see Fig. 1d). Similar to Tanabe, Lavalley and co-workers reported an effect of water on the sulfate species and its IR spectra. They postulated the hydrated sulfate species to have a more ionic sulfate structure attached to only two metal atoms (see Fig. 1e). Morterra *et al.* supported these assignments (11).

The type of acidity present on sulfate-promoted zirconia has been studied using pyridine adsorption. Initially, reports were conflicting about whether Lewis or Brønsted acidity was generated. Some groups reported only Lewis acidity (6) while others reported both types (5, 17). More recently, a number of reports have demonstrated the presence of Brønsted acidity and its importance for catalytic activity (16, 18). The formation of Brønsted acidity was favored at higher sulfate loadings (9, 11, 16, 18), but other factors such as the degree of sample hydration, preparation method, and activation temperature were also important.

The impact of various preparative parameters on the activity of these catalysts has also been studied. Activation temperature (17, 18), preparation method (19), and sulfate content (8, 18) all play an important role in making an active catalyst. For example, the activation temperature required for maximum catalytic activity can change depending on the sulfate source used during impregnation (19).

Two general questions need to be answered to fully understand sulfate-promoted zirconia. First, what is the relationship between preparation and the sulfate structure? Second, how are the acidic, and hence catalytic, properties of these materials affected by the sulfate species on the surface? The links between preparation and structure and between structure and acidity/activity must be found. Our aerogel preparation of zirconia–sulfate materials gives us interesting preparative alternatives to examine these two questions.

Aerogels are high surface area, high porosity materials prepared by the sol–gel method followed by supercritical drying. The first step in the preparation is the formation of an alcogel using sol–gel chemistry. In the sol–gel method (20), a metal alkoxide undergoes hydrolysis and subsequent condensation in an alcohol solvent, forming a polymeric oxide network entraining the alcohol. For catalytic uses, the liquid solvent must be removed from the gel. During conventional drying, a liquid–vapor interface forms in the pores and the corresponding surface tension collapses the oxide network, thereby reducing its surface area. However, in supercritical drying, the liquid solvent is replaced with a supercritical fluid, hence eliminating the liquid–vapor interface. This supercritical fluid can then be safely removed from the pores leaving the oxide network intact. The resulting material is an aerogel. We have previously reported our work on the synthesis and characterization of zirconia aerogels (21).

In this paper, we report the *one-step synthesis* of a sulfate-promoted zirconia aerogel by making a zirconia–sulfate cogel. Instead of first making a zirconia support followed by sulfate impregnation, as is commonly done, we combined the two steps into one by introducing sulfate into the zirconia preparation. During the sol–gel formation of the alcogel, sulfuric acid was added to the zir-

TABLE 1

Zirconia–Sulfate Aerogels: Nomenclature and Sample Data

Sample name	Nominal mol% SO_4^{2-}	Amount H_2SO_4 (ml)	Gel time (sec)	BET surface area[a] (m^2/g)	Pore volume[a] (cc/g)
A-ZrO_2	0	0	20	120	0.348
Series A					
A-ZSO_4 95 #1	5	0.106	45	139	0.322
A-ZSO_4 90 #3	10	0.22	62	145	0.298
A-ZSO_4 80 #1	20	0.50	24	152	0.321
Series B					
A-ZSO_4 95 #2	5	0.106	30	135	0.309
A-ZSO_4 90 #4	10	0.22	50	144	0.307
A-ZSO_4 80 #2	20	0.05	25	155	0.321

[a] For samples calcined at 773 K for 2 h.

conium alkoxide precursor such that sulfate was included in the oxide network of the alcogel, making a zirconia–sulfate cogel.[2] When this cogel was supercritically dried, the resulting product was a zirconia–sulfate aerogel. Another one-step synthesis uses zirconium sulfate as a starting material (22). However, this method does not allow for control of the sulfate content and mixing of the two components.

EXPERIMENTAL

The starting synthetic formulation was that for a standard, undoped zirconia aerogel. The full details of this synthesis can be found elsewhere (21). In summary, a zirconia alcogel was first made. In one beaker, 16.2 ml of zirconium *n*-propoxide (70 wt% in propanol, Alfa) was diluted in a mixture of 15 ml of *n*-propanol (Fisher) and 1.90 ml of HNO_3 (70% w/w, Fisher). In a second beaker, 1.31 ml of distilled water (2.0 mol H_2O/mol Zr^{4+}) was mixed with another 15 ml of *n*-propanol. The water/alcohol mixture was added to the alkoxide/acid/alcohol mixture and stirred with a magnetic stir bar until gelation caused the vortex created by the stirring to disappear. The elapsed time between mixing and the disappearance of the vortex was recorded and called the gel time.

Sulfate ions were introduced in the gelling step. Nominal zirconia–sulfate cogel compositions made were 5, 10, and 20 mol% SO_4^{2-} in ZrO_2 (see Table 1 for nomenclature). Sulfuric acid (95–98%, Certified ACS, Fisher) was used as the sulfate ion source. The required amount of sulfuric acid was added to the alkoxide/acid/alcohol mixture. Since the total acid amount can affect important parameters such as gel time (21), the amount of nitric acid used was reduced such that the total volume of acid was kept at 1.90 ml.

The alcogel was covered with Parafilm and aged for 2 h at room temperature. The alcohol was then removed by supercritical drying with carbon dioxide (23). In a supercritical extraction screening system (Autoclave Engineers, Model 08U-06-60FS), supercritical CO_2 was flowed through the gel at ca. 343 K and 20.7×10^3–24.7×10^3 kPa with a downstream flow rate of 85 liters/h at ambient conditions. The alcohol was completely displaced by CO_2 after approximately 2 h. After removal of the CO_2, the resultant powder, an aerogel, was ground into a power of <100 mesh.

Standard heat treatment consisted of first drying the powder at 383 K for 3 h under a vacuum of 3.4 kPa. This was followed by calcination performed under flowing oxygen (24 liters/h) in a quartz tube inside a tubular furnace. (This calcination step is the *ex situ* activation referred to in the text.) The sample was heated at a rate of 10 K/min to the desired temperature and held at the temperature for 2 h. Samples calcined to 973 and 1173 K were previously calcined to 773 K.

Textural characterization was performed on an Autosorb-1 gas sorption system (Quantachrome Corp.). Samples were first outgassed for 3 h under vacuum at 473 K. Forty-point adsorption and desorption isotherms were obtained, from which BET surface area (taken at $P/P_0 \sim 0.3$), total pore volume (P/P_0 close to unity), and pore size distribution (BJH method) were calculated. Crystal structure determinations were made by X-ray diffraction (XRD) using a Rigaku D/Max diffractometer with CuK_α radiation. Differential thermal analysis (DTA) was performed on a Perkin-Elmer DTA 1700 high-temperature thermal analyzer with thermal analysis data station. A heating rate of 10 K/min was used to heat from room temperature to 1273 K under He flow (3 liters/h). Thermogravimetry was done on a Cahn 113 thermogravimetry microbalance with the weight being electronically processed by a Cahn 2000 recording electrobalance. Approximately 60 mg of sample was heated at 10 K/min from room temperature to 1273 K under flowing He (3 liters/h).

n-Butane isomerization was performed in a differential, downward-flow, fixed-bed catalytic reactor. Approximately 500 mg of catalyst was pretreated under He flow (3 liters/h, Matheson HP) at 588 K for 1 h. The sample was then cooled to 553 K and exposed to the feed stream mixture of hydrogen (1.79 liters/h, Matheson UHP) and *n*-butane (0.079 liters/h, Matheson, CP). A Gow-Mac 550P gas chromatograph with thermal conductivity detector (Column: Supelco 23% SP1700 on 80/20 Chromosorb, 1/8 in. × 13 ft) was used to determine the composition of the product stream.

[2] The polymeric gel network is strictly not an oxide prior to calcination. We use the term zirconia gel mainly to remind us of the calcined product.

A Mattson Galaxy 5020 FTIR with a Harrick diffuse reflection attachment (DRA-2) was used to collect diffuse reflectance infrared (DRIFT) spectra. Spectra were taken using a DTGS detector over a range of 400–4000 cm^{-1} with a resolution of 2 cm^{-1}. Samples were powder-diluted to 2 wt% in KBr. *In situ* DRIFT and pyridine adsorption experiments were performed in a Harrick reaction chamber (HVC-DR2). Samples were pretreated under He flow (3 liters/h) at 588 K for 1 h, then cooled to 553 K to simulate the reaction pretreatment and temperature. Pyridine exposure was carried out at this elevated temperature by diverting the He flow stream through a liquid saturator containing pyridine at room temperature for 15 min. The samples were kept at 553 K for another hour at the end of which a DRIFT spectrum was taken at 553 K. The ratio of Brønsted to Lewis acidity was determined from the spectra of adsorbed pyridine following the method of Basila and Kantner (24). We did not calibrate independently the absolute amounts of Lewis and Brønsted acid sites in our experimental system because our main interest was establishing qualitative trends by comparing data from different samples on a consistent basis.

RESULTS

Textural Properties

Zirconia–sulfate aerogels were made in a one-step process by including sulfate in the gelling step. Sulfuric acid was used in place of a portion of the nitric acid. First, the effect of adding sulfate on the gel time was examined. In our previous work with zirconia (21), we found that gel time was a crucial parameter in determining the aerogel's characteristics. As seen in Table 1, compositions up to 10 mol% SO_4^{2-} increased the gel time, but 20 mol% caused the gel time to decrease again. While there was some variation in gel time with sulfate content, all the gel times fell in the range 20–60 s. These gels were therefore classified in the intermediate gel time range as defined in our previous work (21). Within this range, gel time was not found to have a significant effect on the product's properties. Thus, we attributed differences between these materials to the sulfate content, not to changes in gel time caused by that sulfate content.

After these gels were supercritically dried and calcined, their textural characteristics were determined by nitrogen adsorption. Series A gels were used for most of the textural characterization. Some work was done on Series B gels to check for reproducibility. Surface area and pore volume differences between Series A and B aerogels were less than 5%. Figure 2 shows BET surface area versus sulfate content for the zirconia–sulfate aerogels after four different heat treatments. After calcination

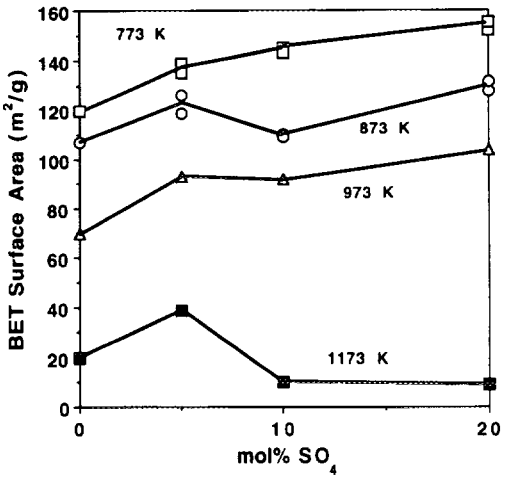

FIG. 2. Effect of heat treatment (calcination for 2 h at the indicated temperature) and sulfate content on surface area. 773 and 873 K data for Series A and B gels. 973 and 1173 K data for Series A only.

at 773 K for 2 h, a pure zirconia aerogel had a surface area of about 120 m^2/g. Adding 5 mol% SO_4^{2-} to the gel increased the surface area to about 135 m^2/g. Further sulfate addition to 10 and 20 mol% SO_4^{2-} increased the surface area to ca. 145 and 150 m^2/g, respectively. An increase in zirconia surface area with the addition of a dopant is commonly seen with both sulfate (5–10) and other additives (25–27). This stabilization did not persist at higher temperatures. The pore volume was relatively insensitive to both sulfate content and heat treatment between calcination temperatures of 773 and 973 K. At these conditions, the pore volume ranged between 0.26 and 0.35 cc/g. However, after 1173 K calcination, the pore volume dropped significantly and became a strong function of sulfate content. Specifically, increasing sulfate loading caused a decrease in pore volume, possibly due to the effect of sulfate decomposition that had occurred by this temperature. These aerogels, after calcination to 773–873 K, were mesoporous with pore size distributions centered around 4.5 to 8.0 nm (see Fig. 3).

Catalytic Properties

The zirconia–sulfate aerogels were tested for their superacidic character by using them as catalysts for *n*-butane isomerization. This reaction requires an acid catalyst at least as strong as 100% sulfuric acid (30), thus making butane isomerization an appropriate test for superacidity. Catalyst performance was examined as a function of both activation temperature (the temperature of the 2-h calcination) and sulfate content. Another gel series (Series B in Table 1) was made to perform these experiments as we were limited in the amount of aerogel

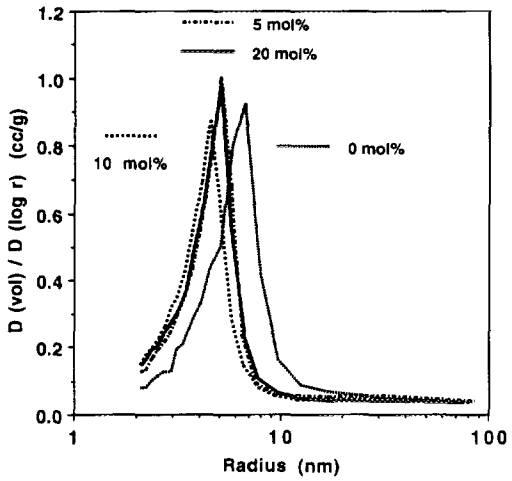

FIG. 3. Pore size distribution for zirconia–sulfate aerogels determined from nitrogen desorption. Mole percent of sulfate is given. Samples were calcined at 773 K for 2 h (Series A gels).

prepared per batch. Figure 4 shows the reaction results for a 10 mol% sulfate cogel at different activation temperatures. All of the catalysts partially deactivated and the degree of deactivation increased with increasing initial rate. The reaction rate reached steady state after 90 min on stream. The initial and final rates, shown in mmol of *n*-butane reacted per gram per hour, are plotted in Fig. 5 versus catalyst activation temperature at different sulfate loadings. Both initial and final rates showed the same qualitative trends for a given sulfate content. The aerogel containing 5 mol% sulfate was inactive at all activation temperatures between 773 and 923 K. The 10 mol% sample (dashed lines in Fig. 5) required heating to 823 K to show catalytic activity. The maximum reaction rate occurred at an activation temperature of 848 K and the rate decreased but remained nonzero up to the maximum tested activation temperature of 923 K. The 20 mol% sample (solid lines in Fig. 5) was active at a lower activation temperature. For this composition, a temperature of only 773 K was sufficient to activate the catalyst. In addition, the maximum reaction rate occurred with an 873-K activation. The 20 mol% SO_4^{2-} sample was active over a broader range of activation temperatures. However, the reaction rate maximum was much sharper. While the maximum rate of the 20-mol% sample was larger than the maximum rate of the 10-mol% sample, at some activation temperatures the 10-mol% sample was more active. Thus, the primary effect of sulfate loading was on the activation behavior of these materials and not on the absolute reaction rates. Surface area variations with sulfate loading and activation temperature (see Fig. 2) were not large enough to account for these reactivity differences. On a per surface area basis, the isomerization rate varied from 5.23 μmol/m^2/h (for 20 mol% SO_4 activated at 873 K after 10 min time on stream) to 0.47 μmol/m^2/h (for 20 mol% SO_4 activated at 773 K after 90 min time on stream). In addition, deactivation was not due to a decrease in surface area because measurements on selected samples before and after butane isomerization showed no change in surface area.

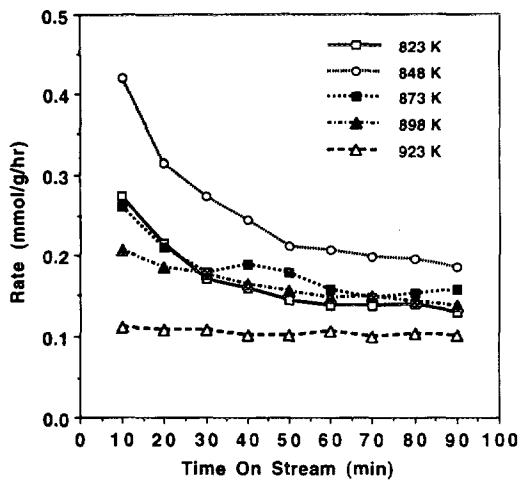

FIG. 4. *n*-Butane isomerization rates vs time on stream for a 10 mol% SO_4^{2-} zirconia–sulfate aerogel (A-ZSO_4 90 #4) at different activation temperatures. Samples were calcined at the indicated temperature for 2 h.

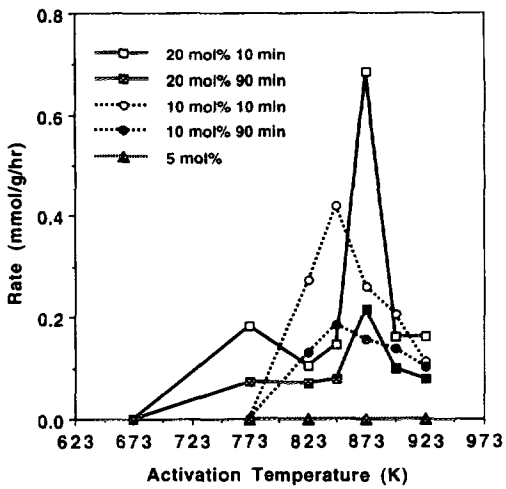

FIG. 5. Effect of activation temperature and sulfate content on *n*-butane isomerization rates for zirconia–sulfate aerogels. Samples were calcined at the indicated temperature for 2 h. The solid lines are for A-ZSO_4 80 #2, the dashed lines for A-ZSO_4 90 #4, and the dotted line is for A-ZSO_4 95 #2. Open symbols represent 10 min on stream; the closed, 90 min.

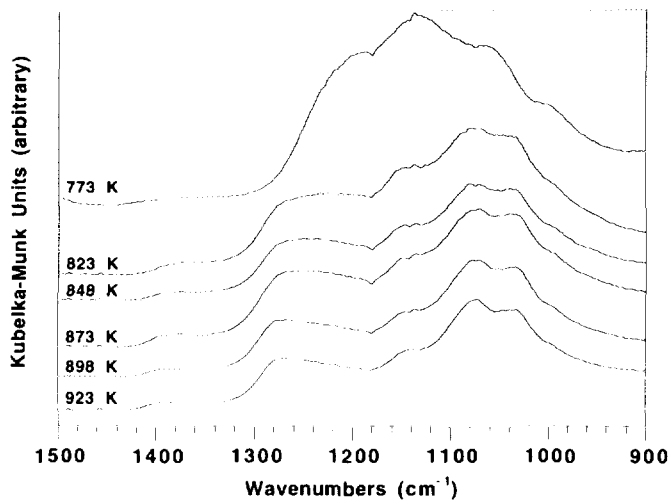

FIG. 6. Diffuse reflectance infrared spectra of a 10 mol% SO_4^{2-} zirconia–sulfate aerogel (A-ZSO_4 90 #4) as a function of activation temperature. Samples were calcined for 2 h at the indicated temperature.

Sulfate DRIFT Spectra

DRIFT spectroscopy was used to help explain the effect of activation temperature on the catalytic activity. Specifically, the sulfate species was seen to undergo changes with increasing heat treatment. Figure 6 shows the sulfate region of *ex situ* DRIFT spectra for a 10 mol% sulfate sample. After 773 K activation, the most intense peak was located at 1137 cm^{-1} with other peaks at 1187, 1064, and 996 cm^{-1}. (The small peak at 1375 cm^{-1} was from the zirconia support as evidenced by a decrease in intensity with increasing sulfate loading). This sample was catalytically inactive. Upon heating to higher temperatures, the peak at 1137 cm^{-1} decreased in intensity and a peak at about 1075 cm^{-1} began to dominate. In addition, a new broad peak at ca. 1270 cm^{-1} was observed which grew slightly with higher activation temperatures. Samples activated to 823 K and above exhibited these DRIFT features and were all catalytically active. In addition, the overall intensity of the sulfate absorption for these active samples decreased from that of the lower activation samples, suggesting a decrease in the amount of sulfate present. In sum, the sulfate species underwent a transition from a low temperature (LT) state (seen in DRIFT by the four overlapping peaks with a maximum intensity at 1137 cm^{-1}) to a high temperature (HT) state (more separated peaks with maximum intensity at 1075 cm^{-1}) with a potential sulfate loss associated with this transition. The hydroxyl region of the DRIFT spectra for this loading showed a large hydroxyl content with significant hydrogen bonding (more details below). In addition, adsorbed molecular water was found on these samples as evidenced by a peak at 1630 cm^{-1} (data not shown).

Similar behavior was seen for the 20 mol% sample (Fig. 7). Samples activated at 848 K or less showed the broad superposition of peaks with a maximum located at 1129 cm^{-1}. Treatment to 873 K or higher brought about the sulfate transition with the largest peak again present at 1070 cm^{-1} and the 1270 cm^{-1} peak growing with increasing activation temperatures. Along with the transition there was a decrease in the sulfate absorbance intensity. The absolute absorbance was constant with activation between 673 and 848 K, but then dropped significantly upon heating to 873 K, which was the activation temperature that gave the maximum rate (Fig. 5). In the 20 mol% sample, the sulfate transition as seen by *ex situ* DRIFT could not be completely correlated with changes in catalytic activity. The sulfate transition occurred between 848 and 873 K, while it only required 773 K activation to generate an active catalyst. However, the reaction rate did increase concurrently with the sulfate transition upon 873 K calcination. The hydroxyl region of the 20 mol% sample was similar to that of the 10 mol% sample discussed above.

This sulfate transition in samples with only 5 mol% sulfate occurred between 673 and 773 K (see Fig. 8). The LT sulfate species had IR peaks very similar to the other zirconia–sulfate samples. (Again, the peak at 1370 cm^{-1} was from the zirconia support.) The HT species, seen over the activation range of 773 to 923 K, had the largest peak centered at 1062 cm^{-1} and other peaks at 1028, 1000, 1125 cm^{-1} and a broad peak at ca. 1240 cm^{-1}. These peaks were about 10–20 cm^{-1} lower than the peaks for

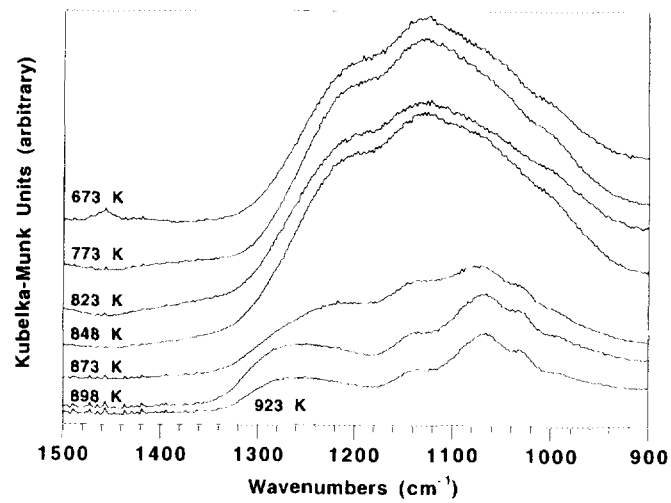

FIG. 7. Diffuse reflectance infrared spectra of a 20 mol% SO_4^{2-} zirconia–sulfate aerogel (A-ZSO_4 80 #2) as a function of activation temperature. Samples were calcined for 2 h at the indicated temperature.

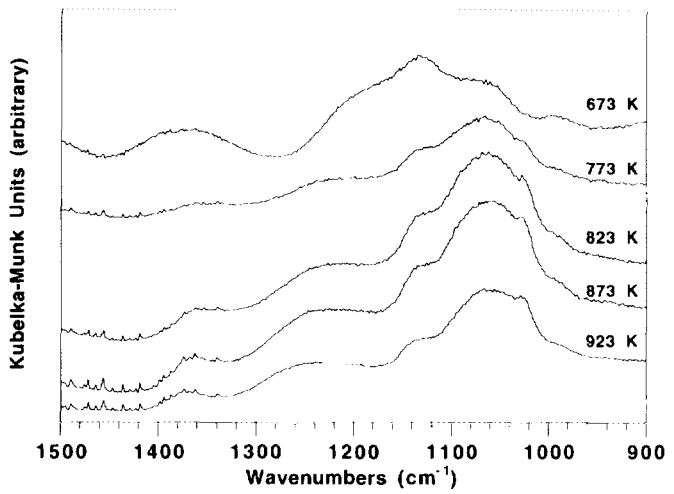

FIG. 8. Diffuse reflectance infrared spectra of a 5 mol% SO_4^{2-} zirconia–sulfate aerogel (A-ZSO_4 95 #2) as a function of activation temperature. Samples were calcined for 2 h at the indicated temperature.

the higher sulfate-loaded aerogels. All of these samples were inactive for *n*-butane isomerization.

Sulfate decomposition was confirmed by examining the DRIFT spectra of aerogels after 1173 K treatment (Series A). The 10 and 20 mol% SO_4^{2-} samples did not show any sulfate IR bands indicating complete removal of sulfur-containing groups. The 5 mol% sample showed some low intensity features in the sulfate IR region, but were very different from any of the lower-temperature samples. This indicated that a small amount of some unknown sulfate species remained after 1173 K calcination on this sample.

The sulfate species and hydroxyl content on the dehydrated surfaces were examined using *in situ* DRIFT. Samples were heated *in situ* to 588 K for 1 h under helium flow and then cooled to 553 K, similar to the pretreatment conditions in the reactor. Figure 9a shows the sulfate region of DRIFT spectra for a 10-mol% sulfate sample. This panel shows the correlation between *ex situ* and *in situ* DRIFT. Curves (1) and (2) are spectra from a catalytically inactive sample which was previously activated to 773 K. Curve (1) was taken at room temperature (*ex situ*). The spectrum consisted of the four overlapping peaks assigned to the LT sulfate species discussed above. Curve (2) was taken *in situ* at a temperature of 553 K. Upon drying, a new peak was formed at about 1350 cm^{-1} and the four broad peaks appeared to shift to lower wavenumbers. All aerogels with sulfate in the LT form behaved in this manner upon drying.

Curves (3) and (4) in Fig. 9a are spectra from a catalytically active 10-mol% sulfate sample previously activated to 848 K. Curve (3), taken at room temperature, showed the sulfate in the HT form. Upon drying, the *in situ* DRIFT spectrum (curve (4)) showed the formation of a new peak at 1380 cm^{-1} and a single broad peak at 1030 cm^{-1}. All aerogels with sulfate in the HT form behaved in a similar manner upon drying. The only exception occurred in the 5 mol% sulfate sample in which the new high wavenumber peak was seen at 1360 cm^{-1} instead of at 1380 cm^{-1}. This observation will be explored below. Differences in the *ex situ* DRIFT spectrum translated into differences in the *in situ* DRIFT spectrum. Thus, *ex situ* DRIFT spectra were a reliable reflection of the *in situ* spectra and therefore related information about the sulfate structure and possible activity of sulfate ions on these catalysts.

In situ DRIFT data gave additional information about the sulfate species itself and its relationship to activity. Aerogels with sulfate in the LT state exhibited a DRIFT peak at about 1350 cm^{-1} or lower at the reaction tempera-

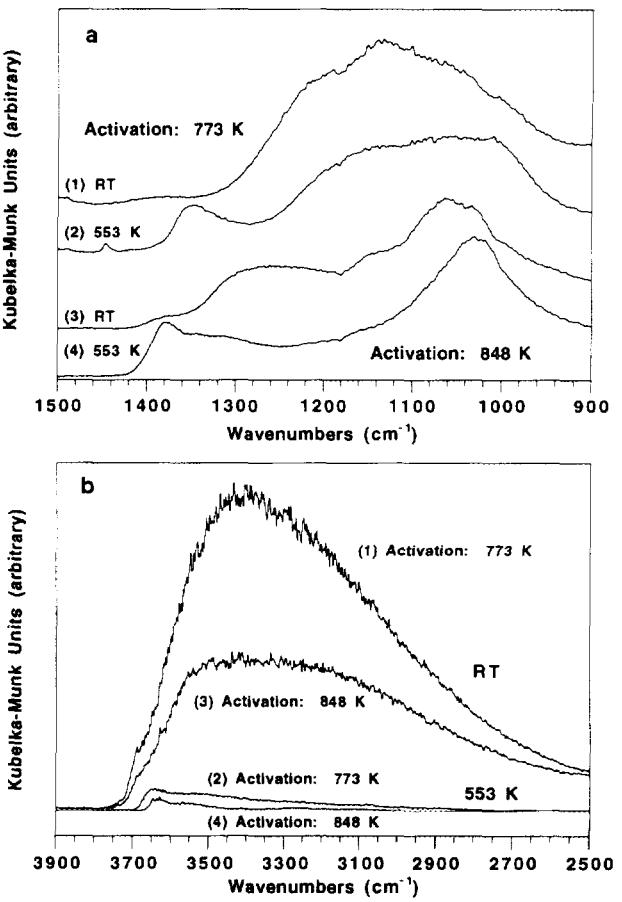

FIG. 9. *In situ* diffuse reflectance infrared spectra for zirconia–sulfate aerogels. (a) Sulfate region of a 10 mol% SO_4^{2-} sample (A-ZSO_4 90 #4). (b) Hydroxyl region of a 10 mol% SO_4^{2-} sample (A-ZSO_4 90 #4). Curve (1): Sample activated at 773 K. Spectrum taken at room temp. Curve (2): Sample activated at 773 K. Spectrum taken at 553 K. Curve (3): Sample activated at 848 K. Spectrum taken at room temp. Curve (4): Sample activated at 848 K. Spectrum taken at 553 K.

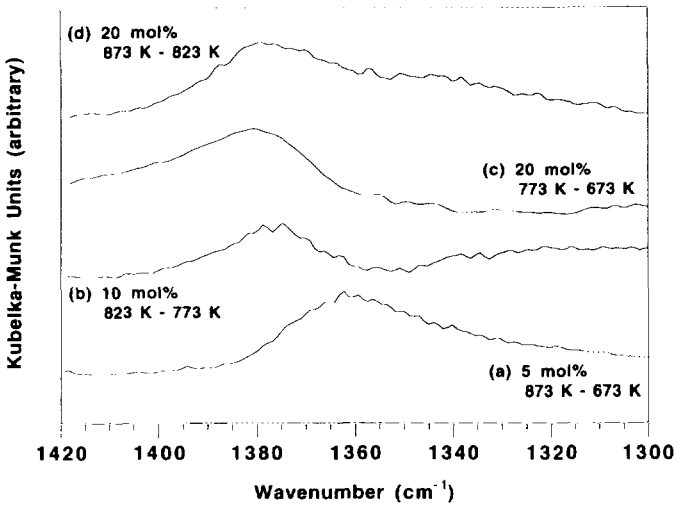

FIG. 10. Difference spectra for zirconia–sulfate aerogels (Series B gels). Original *in situ* diffuse reflectance infrared spectra were taken at 553 K. Example of a spectrum label: (a) "5 mol% 873–673 K" refers to a 5 mol% SO_4^{2-} sample and the spectrum was the result of the 673 K activation spectrum subtracted from the 873 K spectrum. (b)–(d) follow similarly.

ture of 553 K. When the sulfate transformed to the HT state, this DRIFT peak shifted to higher wavenumbers. Subtraction of DRIFT spectra after different activations, as shown in Fig. 10, most clearly shows this transformation from the LT to HT state. Between 773 and 823 K activations in the 10 mol% sample, peak growth occurred at 1380 cm^{-1}. Other changes in activation temperature for the 10 mol% sample showed no significant differences. Similarly, in the 20 mol% sample, peak growth at 1380 cm^{-1} was seen between 673 and 773 K activations as well as between 823 and 873 K activations. Note that these changes in sulfate structure characterized by the 1380-cm^{-1} peak growth also brought about increased catalytic activity. In contrast to the 10 and 20 mol% samples, high temperature activation of a 5-mol% aerogel formed a new peak at only 1360 cm^{-1}. Thus, the catalytically active sulfate species exhibited a peak at 1380 cm^{-1} under dehydrated conditions while inactive sulfate species formed this peak at lower wavenumbers.

Finally, *in situ* DRIFT addressed the issue of hydroxyl content. As discussed above, there was a decrease in hydroxyl content as seen by *ex situ* DRIFT that occurred along with the sulfate transition from the low to high temperature species. In Fig. 9b, curve (1) was an inactive, LT sulfate aerogel while curve (3) was an active, HT sulfate aerogel. The active sample had a lower hydroxyl content. Both samples showed a large amount of hydrogen bonding as evidenced by the broad —OH peak. Upon drying at 553 K, *in situ* DRIFT showed that the hydroxyl content decreased significantly compared to the room temperature spectra (Fig. 9b, curves (2) and (4)). Molecularly adsorbed water was also removed as evidenced by the disappearance of the 1630-cm^{-1} peak (data not shown). Closer examination of the effect of activation temperature on the *in situ* DRIFT hydroxyl region showed that even at elevated temperatures, hydrogen bonding still existed in certain samples. Figure 11 shows the hydroxyl region of the DRIFT spectra, taken at 553 K, of a 20 mol% sulfate sample after different activations. Between 673 and 773 K activation, there was a drop in the *in situ* hydroxyl content, but there was still hydrogen bonding present. Again, between these two activation temperatures, an increase in catalytic activity was seen. Between 823 and 923 K, there was another drop in hydroxyl content with the complete elimination of hydrogen bonding. This temperature range included the large increase in reaction rate that occurred at 873 K (see Fig. 5). Thus, the hydroxyl content and the presence of hydrogen bonding were related in some way to the activation behavior and the activity of these materials.

Thermogravimetry

To further investigate this sulfate transition that occurred with increasing activation temperature, we examined the weight loss of these materials under heating with thermogravimetry (TG). In these experiments, we measured continuously the change in weight during a heat ramp. TG data are shown as a change in weight with time (i.e., a derivative) normalized to the initial weight to account for differing amounts of sample used. Figure 12 shows the effect of sulfate content on the TG curves of

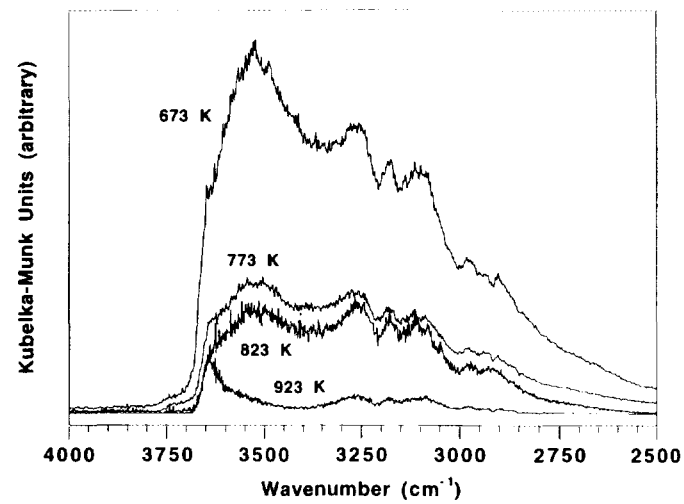

FIG. 11. Hydroxyl region of the *in situ* diffuse reflectance infrared spectra for a 20 mol% SO_4^{2-} zirconia–sulfate aerogel (A-ZSO_4 80 #2) after different activation temperatures. Samples were calcined at the indicated temperature for 2 h. Spectra were taken at 553 K.

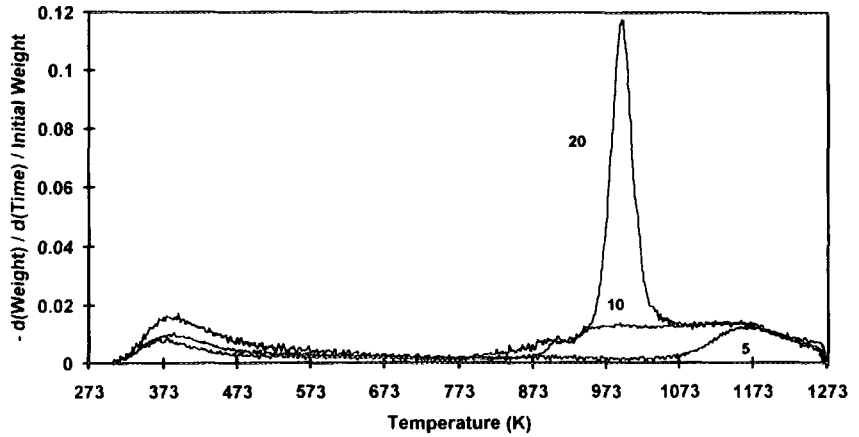

FIG. 12. TG scans of zirconia–sulfate aerogels of different sulfate contents. Samples were calcined to 773 K for 2 h and used as catalysts for butane isomerization (Series B gels). The mol% sulfate is given.

materials previously activated to 773 K and used as an isomerization catalyst. The first weight loss occurred at about 373 K and was most likely due to the desorption of molecular water from the sample. All samples exhibited this weight loss. At higher temperatures there were two modes of weight loss. The first (termed Mode I) had a peak which began at about 873–923 K and had a maximum around 973 K. The second (Mode II) began between 973 and 1073 K with a maximum at ca. 1148 K. We believe that the first mode corresponded to the sulfate transition from the LT to HT sulfate species mentioned above, while the second mode was due to sulfate decomposition.

In the 5 mol% sample, DRIFT showed that the sulfate transition occurred between 673 and 773 K. The TG scan of the 673 K activated aerogel exhibited a Mode I peak at 873 K (see Fig. 13). The 773 K activated sample did not show this peak, indicating that the transition occurred between the 673 and 773 K activations (as supported by DRIFT). The second weight loss (Mode II), starting at 1073 K, was assigned to sulfate decomposition and occurred for all activations.

For the 10 mol% sample, the transition took place at a slightly higher activation temperature (DRIFT showed between 773 and 823 K). The sample activated to 773 K showed a small amount of the Mode I weight loss starting at 873 K followed by Mode II weight loss (see Fig. 14). Samples run after higher activation temperatures showed weight losses starting at higher temperatures due to Mode II only. The sulfate transition (or Mode I) had already occurred in the activation step for these samples.

The 20 mol% sample showed the Mode I weight loss most clearly (Fig. 15). Activations up to and including 823 K showed a large peak for Mode I. This peak decreased in size with activation to 848 and 873 K. While DRIFT showed that the sulfate transition had occurred

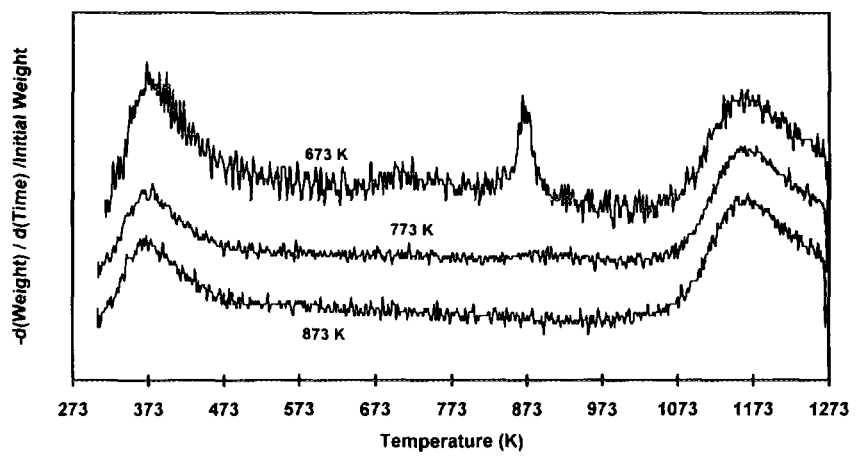

FIG. 13. TG scans of a 5 mol% SO_4^{2-} zirconia–sulfate aerogel (A-ZSO_4 95 #2) after different activation temperatures. Samples were calcined at the indicated temperature for 2 h and used as a catalyst for butane isomerization.

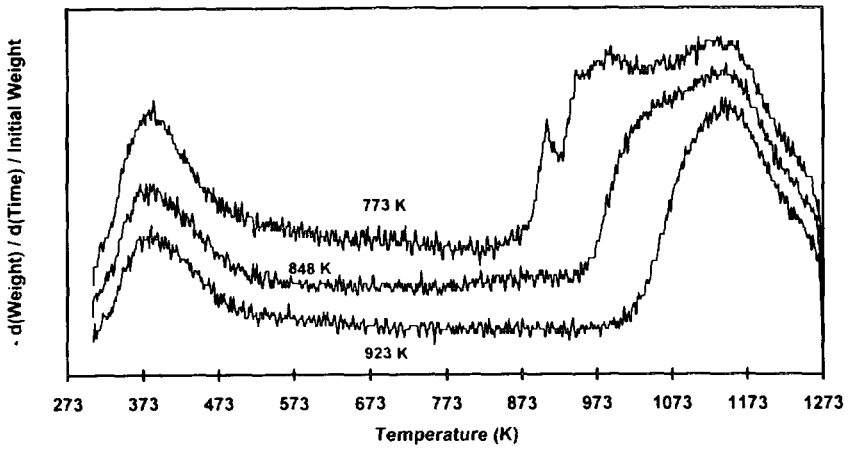

FIG. 14. TG scans of a 10 mol% SO_4^{2-} zirconia–sulfate aerogel (A-ZSO_4 90 #4) after different activation temperatures. Samples were calcined at the indicated temperature for 2 h and used as a catalyst for butane isomerization.

after 873 K activation, there was still a small transition-mode peak (Mode I) remaining in the TG scan. Activation to 923 K and above showed only Mode II weight loss. In addition, activation to only 673 K showed a third mode of weight loss between 773 and 873 K in the TG run. This third mode, which was seen in the 673-K activated sample but not in the 773 K activation, corresponded to the generation of activity which was seen in the 773-K activated sample. The TG data supported the DRIFT data in that there was a loss of sulfate that accompanied the sulfate transition from the low- to high-temperature state.

Crystal Structure

Crystal structure determinations were made by X-ray diffraction (see Fig. 16). At 773 K, pure zirconia crystallized into the tetragonal phase. Further heat treatment caused the tetragonal phase to transform to the monoclinic phase, with virtually 100% transformation by 1173 K. The addition of sulfate retarded both the initial amorphous-to-tetragonal crystallization as well as the tetragonal-to-monoclinic transformation. Addition of 10 mol% or more of sulfate prevented the aerogel from crystallizing at 773 K. Heating to 823 and 848 K was required to crystallize the 10 and 20 mol% SO_4^{2-} samples, respectively. In addition, after 973 K calcination, while pure zirconia was a mixture of the tetragonal and monoclinic phases, all of the samples with sulfate were pure tetragonal. However, all samples heated to 1173 K had transformed to the monoclinic phase. Sulfate, which had retarded the transformation, had decomposed by this temperature. It was noted that the 5 and 10 mol% aerogels crystallized at the same activation temperatures at which the sulfate transition was seen to occur. For example, the 10 mol% sulfate composition was X-ray amor-

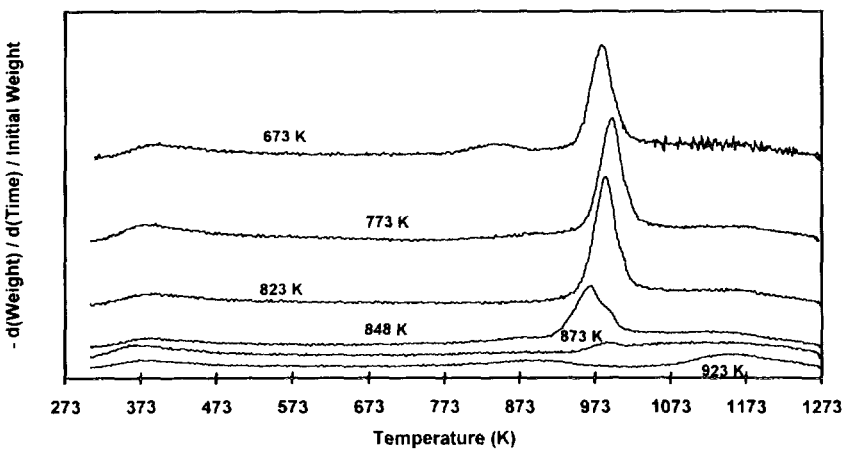

FIG. 15. TG scans of a 20 mol% SO_4^{2-} zirconia–sulfate aerogel (A-ZSO_4 80 #2) after different activation temperatures. Samples were calcined at the indicated temperature for 2 h and used as a catalyst for butane isomerization.

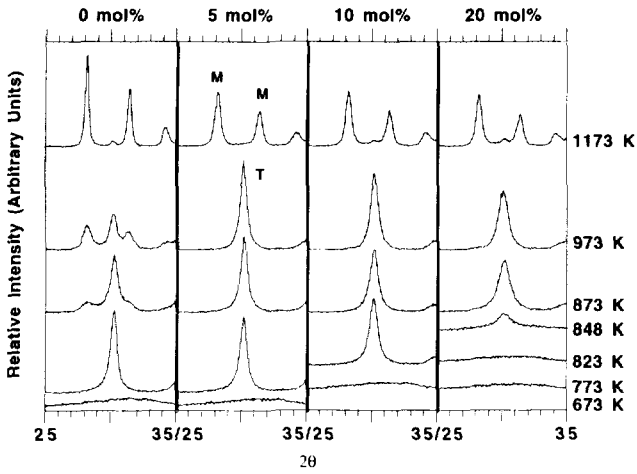

FIG. 16. X-ray diffraction patterns for zirconia–sulfate aerogels vs sulfate content and heat treatment. T and M denote the characteristic peaks of the tetragonal and monoclinic phases of zirconia, respectively. Samples were calcined at the indicated temperature for 2 h (Series A and B gels).

phous at 773 K. This sample, under DRIFT, showed the LT form of the sulfate ion. Upon heating to 823 K, the aerogel crystallized into the tetragonal phase and the sulfate species converted to the HT form as seen by DRIFT. Similar behavior was seen in the 5 mol% sample. The 20 mol% composition differed only in that the 848 K sample, which showed the LT sulfate structure in DRIFT, was weakly crystalline. But, activation to 873 K yielded a fully crystalline aerogel and a completed sulfate transition. Crystallization and the sulfate transition appeared to occur after the same activations, and the retardation of this activation temperature was a function of sulfate content.

The retardation of the initial amorphous-to-tetragonal crystallization was also clearly observed in differential thermal analysis (DTA). DTA scans were performed on the vacuum dried samples before calcination. An exothermic peak in the range of 773–873 K corresponded to the crystallization of zirconia into the tegragonal phase. As sulfate was added, this peak shifted to higher temperatures and broadened. This phenomenon has been reported previously for other preparation methods (6, 7, 12). For a pure-zirconia aerogel, this peak was located at ca. 773 K. For the zirconia–sulfate aerogels of 5, 10, and 20 mol% sulfate, the peak was located at ca. 831, 891, and 910 K, respectively. These temperatures were very close to the onset temperature of the Mode I weight loss exhibited in the TG scans. This provided more evidence that the Mode I weight loss, which was due to the sulfate transition, occurred upon the crystallization of the zirconia support.

Brønsted versus Lewis Acidity

To explore whether the type of acidity present was a determining factor in these materials, we used DRIFT to examine the spectra of adsorbed pyridine, which can differentiate between Brønsted and Lewis acidity (24). Selected samples were tested before and after their use as a catalyst and it was found that the reaction had no effect on the Brønsted to Lewis ratio. Samples were pretreated to 588 K for 1 h under flowing helium, as they were treated before reaction, and then cooled to the reaction temperature of 553 K and exposed to pyridine. A numerical ratio of Brønsted to Lewis acidity was determined from the peak areas of the 1445 and 1490 cm^{-1} peaks due to adsorbed pyridine (24). The effect of activation temperature on the Brønsted to Lewis acidity ratio (solid lines) for these aerogels is shown in Fig. 17 along with the corresponding initial reaction rates (dashed lines). Figure 17a shows the acidity ratio for the 10 mol% sample. After 773 K activation, the sample had only Lewis acidity and was not catalytically active. However, calcination to 823 K created Brønsted acidity in addition to Lewis acidity. This sample was catalytically active. Increased heat treatment reduced the Brønsted to Lewis ratio, but Brønsted acidity remained even after 923 K activation.

The 20 mol% sample (Figure 17b) showed similar results. The 673 K activated sample was catalytically inactive and contained only Lewis acidity. Higher temperature activation formed Brønsted sites and these samples were active for isomerization. The 5 mol% sample, after a heat treatment of 873 K, showed no Brønsted acidity and was an inactive catalyst. Thus, Brønsted acidity was required for an active *n*-butane isomerization catalyst.

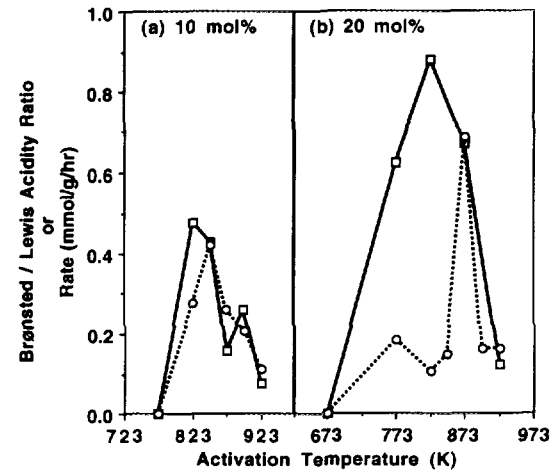

FIG. 17. Brønsted to Lewis acidity ratios for (a) 10 mol% SO_4^{2-} and (b) 20 mol% SO_4^{2-} zirconia–sulfate aerogels. Samples were calcined at the indicated temperature for 2 h. The solid lines represent the acidity ratio. The dashed lines represent the *n*-butane isomerization rates after 10 min on stream, which are given for reference.

Higher sulfate contents favored the formation of Brønsted acidity. But, there was not always a direct correlation between the acidity ratio and the overall reaction rate (see Fig. 17b).

DISCUSSION

In the previous section, we presented a large amount of data on these zirconia–sulfate aerogels. To bring these results together, we will first present a model for the effect of heat treatment and sulfate loading on these materials and their properties. Then, we will cite the experimental evidence that supports this model. We start by examining the 10 mol% sulfate aerogel.

A-ZSO$_4$ 90, 773 K and Below

Sulfate was included during the sol–gel synthesis step causing the sulfate to be placed into the growing gel network. Sulfate was present throughout the bulk of the material, not necessarily at the surface. The presence of sulfate in the gel network acted to retard the crystallization of zirconia into the tetragonal phase upon calcination. Thus after low-temperature activations (773 K and lower) the aerogel was still X-ray amorphous. The sulfate groups were present in an inactive state (the LT species) and buried inside the bulk of the aerogel (see Fig. 18). This buried, inactive sulfate group was partially ionic with a reduced S=O bond order of less than two. The surface of the material was not yet chemically modified by the sulfate ions and acted as pure zirconia: it contained only Lewis acidity and was inactive for *n*-butane isomerization. There was a large population of hydrogen-bonded hydroxyl groups. Even upon drying, hydroxyl groups remained in a hydrogen-bonded environment.

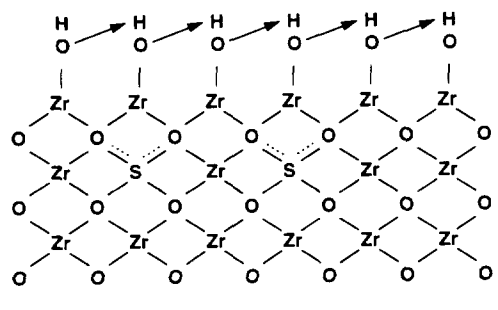

FIG. 18. Schematic diagram of a zirconia–sulfate aerogel. Sulfate is located in the bulk of the aerogel with none on the surface. The sulfate is in the low temperature (LT) state. The aerogel is X-ray amorphous. Representative samples would be A-ZSO$_4$ 95 #2 activated to 673 K, A-ZSO$_4$ 90 #4 activated to 773 K, and A-ZSO$_4$ 80 #2 activated to 673 K. The diagram is not intended to be an accurate representation of actual atomic linkages. Arrows represent hydrogen bonding.

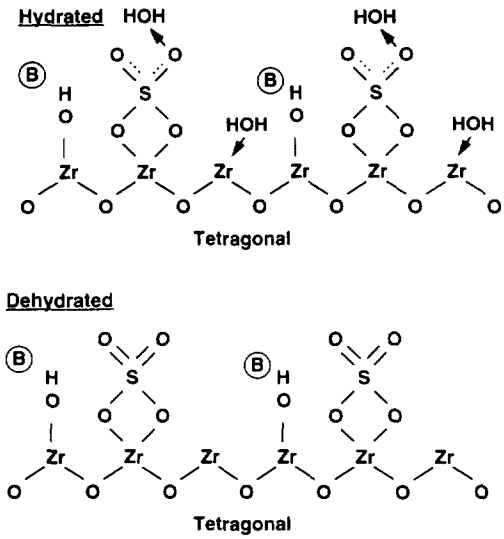

FIG. 19. Schematic diagram of a zirconia–sulfate aerogel. The zirconia is tetragonal and sulfate is located on the surface. The sulfate is in the high temperature (HT) state. The upper panel represents a hydrated (*ex situ*) sample while the lower panel represents a dehydrated (*in situ*) sample. Representative samples would be A-ZSO$_4$ 90 #4 activated to 823 K and A-ZSO$_4$ 80 #2 activated to 873 K. The diagram is not intended to be an actual representation of complete atomic linkages. Arrows represent hydrogen bonding. B denotes a Brønsted acid site.

A-ZSO$_4$ 90, 823 K

Heating to 823 K for 2 h was severe enough to cause the crystallization of the zirconia support. This crystallization had a number of effects. The sulfate in the bulk was expelled onto the surface of the material. During this process, some sulfate was lost and some dehydroxylation occurred. Now at the surface, the sulfate transformed into an active HT species (see Fig. 19). These factors allowed for the formation of strong Brønsted acidity. On a dehydrated sample, the protons were from free hydroxyl groups on the zirconia surface located near "activated" sulfate groups. The activated sulfate groups, now more strongly covalent in nature, contained S=O bonds with a bond order close to 2. These double bonds had an electron-inductive effect, strengthening the proton donating ability of the zirconia surface. The regular crystal structure of the support helped in the charge transfer and delocalization. The Brønsted sites formed were strong enough to catalyze *n*-butane isomerization.

A-ZSO$_4$ 90, Higher Temperatures

Activation to higher temperatures began to degrade the surface and decrease Brønsted acidity and reaction rate. This was probably caused by the decomposition of some sulfate groups as well as the loss of some surface hydroxyls. As long as sulfate was present, the tetragonal-to-

monoclinic transformation was retarded. However, when all the sulfate was removed after 1173 K calcination for 2 h, the sample converted to the monoclinic form.

A-ZSO$_4$ 95, 673 K

The 5 mol% sulfate sample activated to 673 K was very similar to the 10 mol% sample activated to 773 K. The sulfate was in the inactive form located in the bulk (Fig. 18). The surface was not chemically modified (inactive, only Lewis acidity) and the material was X-ray amorphous.

A-ZSO$_4$ 95, 773 K and Higher

Differences between the 5 and 10 mol% samples began to occur at 773 K activation. Since the 5 mol% sample contained less sulfate, it was less effective in retarding crystallization. Crystallization occurred after 773 K for 2 h, expelling the sulfate onto the surface. The sulfate transformed into the HT state. However, this sample, despite these facts, did not catalyze the isomerization reaction. There were too few sulfate groups present on the surface to form Brønsted acidity. Apparently, a certain "critical density" of sulfate must be surpassed in order to generate an active catalyst.

A-ZSO$_4$ 80, 673 K

Again, as with the 5 and 10 mol% sulfate samples, the 20 mol% sample, after low-temperature activation, contained all the sulfate in the inactive LT form located in the bulk. The aerogel was X-ray amorphous, possessed only Lewis acidity, and was inactive.

A-ZSO$_4$ 80, 773 K

Like the 10-mol% sample, this aerogel contained enough sulfate in the bulk to prevent the zirconia from crystallizing after 773 K calcination for 2 h. However, the sulfate content in this material was large enough that due to sintering and other factors, some sulfate was expelled onto the surface (see Fig. 20), and a small amount was lost in the process. Some of these sulfate groups transformed to the HT state with more strongly covalent S=O double bonds. These sulfate groups were capable of forming Brønsted acidity strong enough to catalyze the isomerization reaction. However, the majority of the Brønsted sites formed were weak. Most of the surface sulfate groups were still in the inactive LT form with weak electron induction potential. In addition, the hydroxyl groups present, even at reaction temperatures, were still participating in hydrogen bonding, inhibiting their ability to donate a proton. Weak Brønsted sites were also formed from the protons on the inactive sulfate groups. Thus, the increased sulfate loading of this sample

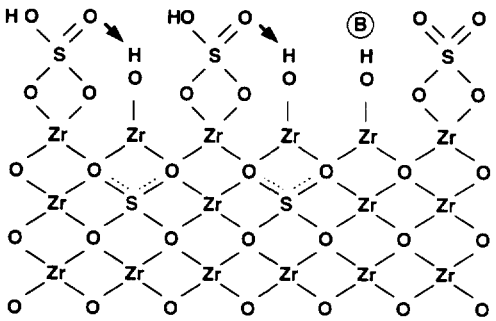

FIG. 20. Schematic diagram of a zirconia–sulfate aerogel. The zirconia is X-ray amorphous and sulfate is located both on the surface and in the bulk. The surface sulfate is a mix of high (HT) and low (LT) temperature forms. This sample is in the dehydrated (*in situ*) state. A representative sample would be A-ZSO$_4$ 80 #2 activated to 773 K. The diagram is not intended to be an actual representation of complete atomic linkages. Arrows represent hydrogen bonding. B denotes a Brønsted acid site.

created a large number of Brønsted sites, but this same increased loading interfered with the strengthening of those sites.

A-ZSO$_4$ 80, 823 and 848 K

The large sulfate content of this material prevented crystallization even after 823 K. The zirconia support began to crystallize after 848 K calcination. The partial crystallization expelled some of the sulfate groups to the surface allowing them to transform into the HT state and causing the loss of some sulfate, but the amount transformed did not affect the chemical behavior of the surface.

A-ZSO$_4$ 80, 873 K

Finally, after 873 K activation, the aerogel was fully crystalline. The majority of the sulfate had been expelled onto the surface where it had been able to transform completely into the HT state. The activated sulfate species, with covalent S=O double bonds, had the electron withdrawing effect to strengthen the Brønsted sites. Sulfate was again lost in the transition and some dehydroxylation occurred. No hydrogen bonding existed under reaction conditions to inhibit proton donation. These conditions (the activated HT sulfate state, the crystalline support, and lack of hydrogen bonding) acted together to strengthen the Brønsted sites to give a higher reaction rate.

In sum, here are the key features of the model. (1) Sulfate, located in the bulk, acts to retard the crystallization. The larger the sulfate content, the higher the temperature required to form a crystalline support. (2) Crystallization expels sulfate onto the surface of the support allowing for the sulfate to transform from an inactive to

an activated species. (3) There is a critical density (or loading) of sulfate ions required to form the Brønsted acidity needed for *n*-butane isomerization. Let us more closely examine how the data support this model.

We clearly saw two sulfate states with DRIFT (see Fig. 9a). The primary differences were the shape and intensities of the peaks located between 1270 and 1000 cm^{-1} and the location of the S=O peak in the dehydrated state. The LT species consisted of four overlapping peaks from 1250–1000 cm^{-1} and were the same regardless of sulfate content. When dehydrated, an S=O peak (specifically an S=O asymmetric stretch (13)) formed at ca. 1350 cm^{-1}. The HT species showed different peak intensities and locations between 1270 and 1000 cm^{-1}. In addition the dehydrated sample exhibited the S=O peak at 1380 cm^{-1} for 10 and 20 mol% samples (1360 cm^{-1} for 5 mol%). This shift in the location of the S=O peak to higher wavenumbers can be related to an increase in the covalent character and bond order of the sulfate group (13). Very similar "dehydrated" activated spectra were reported by both Tanabe (13) and Lavalley (15). However, the assignment of sulfate structure to this spectrum was very different between these two groups (Figs. 1b and 1c). Our work does not address the determination of the actual sulfate structure. However, the important factor is the presence of the S=O bond in the activated species, which acts as an electron inductor (13). The activated HT sulfate species consisted of covalent S=O double bonds while the LT state had more ionic character, less inductive potential, and hence was an inactive catalyst.

The activated HT sulfate species, and hence maximum catalytic activity, only occurred on a tetragonal zirconia. For all three compositions, the activated HT sulfate species as seen by DRIFT occurred only on samples which were fully tetragonal (Fig. 16). First, crystallization caused the expulsion of sulfate to the surface of the material, allowing the sulfate to be accessible for reaction. During this expulsion, some sulfate was lost as seen by the Mode I weight loss TG peak. In other words, the Mode I TG weight loss corresponded to the conversion of the LT inactive sulfate species into the HT activated sulfate species. Samples with larger sulfate contents lost more sulfate as seen by the increasing size of the Mode I peak with sulfate content (see Figs. 12–15). Second, the activated sulfate species could only form on a regular crystal surface. For example, a 20 mol% sample activated to 773 K was X-ray amorphous, had a small degree of catalytic activity, and contained Brønsted acidity. Some of the surface sulfate was activated as evidenced by its ability to catalyze the isomerization reaction and the formation of the 1380-cm^{-1} DRIFT peak (Fig. 10c). These sulfate groups were probably formed on crystallites that were too small to be detected by X-ray diffraction but that would be expected to exist given the high heating temperature. However, the majority of surface sulfate ions were located on amorphous zirconia in an inactive LT state forming weak Brønsted sites not capable of catalyzing the reaction. After crystallization at 873 K activation, the majority of sulfate transformed into the HT activated state and the reaction rate increased significantly. Other work in the literature also points to the importance of a crystalline support for maximum activity (9, 11, 28, 29). Morterra *et al.* (28) reported the presence of Brønsted sites (the type of acidity required for isomerization in our work) only when sulfate was present on regular patches of low-index crystal planes. When sulfate was present on crystallographic defects, no Brønsted acidity was formed. In addition, a regular crystal structure might help charge transfer and delocalization (29).

Crystallization also affected activity due to the dehydroxylation of the zirconia surface. Hydrogen bonding acted to inhibit the ability of an —OH group to donate its proton. Upon the crystallization of zirconia, dehydroxylation occurred on the surface and the amount of hydrogen bonding decreased (Fig. 11, 823 K → 923 K). Some of the remaining free hydroxyl groups were then converted into Brønsted sites as the protons were no longer participating in hydrogen bonding and were more easily donated. We propose that the active Brønsted sites were free hydroxyl groups located near activated HT sulfate ions such that the electron withdrawing effect of the sulfate ions made proton donation easier. The regular crystal network facilitated this electron transfer. These factors combined to cause a sharp increase in reaction rate upon support crystallization.

There were two primary effects of sulfate loading: the retardation of crystallization and the density of sulfate groups. Larger sulfate contents retarded the crystallization to higher temperatures (Fig. 16). Thus, different activation temperatures were required to "activate" the aerogel depending on sulfate composition (note different reaction rate maxima versus activation temperature for 10 mol% versus 20 mol% in Fig. 5). The reasons for this have already been discussed. In addition, sulfate content played a role in the number and type of sites generated. A certain "minimum" threshold of sulfate density was required to generate Brønsted acidity. We propose that the 5-mol% sulfate sample did not contain enough sulfate groups to provide a "group inductive" effect to generate Brønsted sites out of surface hydroxyls, despite the fact that the sulfate was in the activated HT state on a crystalline support. Another possibility is that given the low sulfate loading and the reduced population of hydroxyl groups due to dehydroxylation, no sulfate and hydroxyl groups were located close enough to generate strong acidity. The 10 and 20 mol% samples passed the critical threshold and were able to generate active Brønsted sites (see Fig. 17). The peak positions in the DRIFT spectra

might be an indicator of which samples exceed the required density and which do not. In the 5 mol% sample, the S=O peak in the dehydrated HT sulfate species after 873 K activation (see Fig. 10a) was seen at 1360 cm^{-1}. In the active 10 and 20 mol% samples, this peak was seen at 1380 cm^{-1}. Lavalley *et al.* (15) reported similar results in that increasing sulfate loading caused this peak to shift to higher wavenumbers. In addition, the *ex situ* DRIFT spectrum of our inactive 5 mol% aerogel showed the HT sulfate peaks were about 10–20 cm^{-1} lower than those for the active higher sulfate loadings. In other words, the active and inactive sulfate species have distinct DRIFT fingerprints.

Our data do not support the existence of a polysulfate active species similar to S_2O_7 like Fig. 1d on our aerogels. This structure was reported to have an S=O peak at above 1400 cm^{-1} (11, 15). We never saw a peak above this wavenumber. In addition, increasing sulfate loading led to a larger sulfate loss during the transition from the low- to high-temperature species. This would not be expected if larger sulfate loadings were to form large polysulfate species (i.e., the extra sulfate would form large sulfate species, not be lost in the transition).

Our model can explain other literature results. The formation of Brønsted acidity has been shown to be favored at higher sulfate loadings. For example, Lavalley and coworkers found that large amounts of sulfate impregnated by ammonium sulfate created Brønsted acidity and dramatically increased the activity of the catalyst (16). Our model would predict this in that a large amount of impregnated sulfate would surpass the "critical density" of sulfate required on the surface to form Brønsted acidity. In addition, our model shows that crystallinity of the zirconia support is required for the most active catalysts. An example is found in the work of Chen *et al.* (9). They found a significant increase in *n*-butane isomerization between activations of 673 and 773 K which also corresponded to crystallization of the tetragonal phase.

CONCLUSIONS

We have developed a one-step synthesis for the production of sulfate-promoted zirconium oxide. The inclusion of sulfate ions in the sol–gel formation of zirconia–sulfate cogels, followed by supercritical drying, formed a zirconia–sulfate aerogel. From this synthesis, we saw the importance of a number of preparative variables on the structure and activity of these catalysts.

Our zirconia–sulfate aerogels had a surface area in the range of 135–155 m^2/g, varying with sulfate content, after calcination at 773 K for 2 h. The sulfate content had many effects on the aerogels, the most important of which was the effect on activation behavior. Increased sulfate content retarded the amorphous-to-tetragonal crystallization of zirconia. This crystallization was required to expel the sulfate onto the surface of the oxide where the sulfate was then able to transform into an activated state for a high *n*-butane isomerization rate. Thus, the activation temperature to yield an optimized catalyst changed with sulfate content. In addition, increased sulfate content above a critical threshold increased the ability of the aerogel to form Brønsted acidity, which was required for *n*-butane isomerization.

The sulfate species existed in two states. At low activation temperatures before the crystallization of the support, the sulfate was partially ionic in nature with the S=O bond order less than two. At higher temperatures, the sulfate transformed into a more strongly covalent species with S=O bond orders close to two. This high temperature species provided an electron withdrawing capability that increased the Brønsted strength of the zirconia surface. The transformation between these two species was related to the crystallization of the zirconia support.

In sum, the preparation method is critically important. Because changes in preparation method can affect the type of acidity present and the optimal activation temperature of solid superacids, a comparison of literature results is meaningful only on properly characterized materials.

ACKNOWLEDGMENTS

This work was supported by the National Science Foundation (CTS-9200665). D.A.W. thanks the Texaco Foundation for the support of a graduate fellowship. We also thank Jim Miller for this help with the butane isomerization.

REFERENCES

1. Yamaguchi, T., *Appl. Catal.* **6,** 1 (1990).
2. Hino, M., Kobayashi, S., and Arata, K., *J. Am. Chem. Soc.* **101,** 6439 (1979).
3. Olah, G. A., Surya Prakash, G. K., and Sommer, J., "Superacids." Wiley, New York, 1985.
4. Arata, K., *Adv. Catal.* **37,** 165 (1990).
5. Sohn, J. R., and Kim, H. W., *J. Mol. Catal.* **52,** 361 (1989).
6. Yamaguchi, T., Tanabe, K., and Kung, Y. C., *Mater. Chem. Phys.* **16,** 67 (1986).
7. Scurrell, M. S., *Appl. Catal.* **34,** 109 (1987).
8. Parera, J. M., *Catal. Today* **15,** 481, (1992).
9. Chen, F. R., Coudurier, G., Joly, J.-F., and Vedrine, J. C., *J. Catal.* **143,** 616 (1993).
10. Srinivasan, R., Taulbee, D., and Davis, B. H., *Catal. Lett.* **9,** 1 (1991).
11. Morterra, C., Cerrato, G., Emanuel, C., and Bolis, V., *J. Catal.* **142,** 349 (1993).
12. Srinivasan, R., and Davis, B. H., *Prepr. Div. Pet. Chem. Am. Chem. Soc.* **36,** 635 (1991).
13. Jin, T., Yamaguchi, T., and Tanabe, K., *J. Phys. Chem.* **90,** 4794 (1986).

14. Yamaguchi, T., Jin, T., and Tanabe, K., *J. Phys. Chem.* **90,** 3148 (1986).
15. Bensitel, M., Saur, O., Lavalley, J.-C., and Morrow, B. A., *Mater. Chem. Phys.* **19,** 147 (1988).
16. Waqif, M., Bachelier, J., Saur, O., and Lavalley, J.-C., *J. Mol. Catal.* **72,** 127 (1992).
17. Hino, M., and Arata, K., *J. Chem. Soc., Chem. Commun.* 851 (1980).
18. Nascimento, P., Akratopoulou, C., Oszagyan, M., Coudurier, G., Travers, C., Joly, J. F., and Vedrine, J. C., *Stud. Surf. Sci. Catal.* **75** (New Frontiers in Catalysis), 1185 (1993).
19. Tanabe, K., Yamaguchi, T., Akiyama, K., Mitoh, A., Iwabuchi, K., and Isogai, K., in "Proceedings, 8th International Congress on Catalysis, Berlin, 1984," Dechema, Frankfurt-am-Main, 1984.
20. Brinker, C. J., and Scherer, G. W., "Sol–Gel Science: The Physics and Chemistry of Sol–Gel Processing." Academic Press, Boston, 1990.
21. Ward, D. A., and Ko, E. I., *Chem. Mater.* **5,** 956 (1993).
22. Arata, H., Hino, M., and Yamagata, N., *Bull. Chem. Soc. Jpn.* **63,** 244 (1990).
23. Cheng, C.-P., Iacobucci, P. A., and Walsh, E. N., U.S. Patent 4,619,908, Oct. 28, 1986.
24. Basila, M. R., and Kantner, T. R., *J. Phys. Chem.* **70,** 1681 (1966).
25. Mercera, P. D. L., van Ommen, J. G., Doesburg, E. B. M., Burggraaf, A. J., and Ross, J. R. H., *Appl. Catal.* **71,** 363 (1991).
26. Soled, S., and McVicker, G. B., *Catal. Today* **14,** 189 (1992).
27. Miller J. B., Rankin, S. E., and Ko, E. I., *J. Catal.*, **148,** 673 (1994).
28. Morterra, C., Cerrato, G., and Bolis, V., *Catal. Today* **17,** 505 (1993).
29. Ishida, T., Yamaguchi, T., and Tanabe, K., *Chem. Lett.*, 1869 (1988).
30. Jacobs, P., *in* "Characterization of Heterogeneous Catalysts" (F. Delannay, Ed.), p. 367. Dekker, New York, 1984.